ChemistrySelect

Research Article
doi.org/10.1002/slct.202503439

Chemistry Europe
European Chemical Societies Publishing

www.chemistryselect.org

Schiff Base Thin Film Materials for Chloroform Vapor Detection

Rifat Çapan,*[a] Dilek Öğrence,[a] and Hilmi Namli[b]

Two novel Schiff base compounds, (E)-4-((4-(dimethylamino)-benzylidene)amino)benzoic acid (**DMPABA**) and (E)-4-(2-(4-(dimethylamino)benzylidene)hydrazinyl)benzoic acid (**DMPHBA**), were synthesized to investigate for the vapor sensor behavior against chloroform vapor. **DMPABA** and **DMPHBA** thin films were fabricated using the spin coating method. A surface plasmon resonance system was employed to study the sensor response and the adsorption behavior. The Elovich model was chosen to determine the initial adsorption rate (*a*) and the Elovich desorption constant (*b*). Sensor response rates of **DMPHBA** and **DMPABA** thin films were determined to be 8.38 and 6.93, respectively. The *a* values of the **DMPHBA** and **DMPABA** thin films were calculated as 2775.97 and 1728.51 ppm mm^{-2}, respectively. The *b* value (0.0373 mm^2s ppm^{-1}) of the **DMPHBA** thin film was lower than the *b* value (0.0602 mm^2s ppm^{-1}) of the **DMPABA** thin film. The **DMPHBA** film against chloroform vapor yielded a better performance than the **DMPABA** thin film. The chemical difference between the two materials is an —NH— group, which improved the sensor response and adsorption behavior.

1. Introduction

Volatile organic compounds (VOCs) with low molecular weights are easily evaporated at room temperature and are one of the major air pollutants. There are increasing efforts toward the design and synthesis of new molecules to detect and identify VOCs at room temperature. Different types of organic materials, such as porphyrins,[1] phthalocyanine,[2] calixarene,[3] conjugated polymers,[4] and metal organic frameworks (MOFs),[5,6] fabricated as thin film sensors have been extensively studied for their VOCs sensing properties. There is limited information in the literature on the study of Schiff base material produced as a thin film VOC sensor using the spin coating deposition technique.[7–9] Schiff base materials are significant candidates in the development of VOC sensors due to the imine (—C═N—) group that breaks the molecular symmetry, the conjugation, their amphiphilic nature, and electronic properties.[10,11]

The imine nitrogen atoms acting as Lewis bases in Schiff base compounds interact with the target species via various electrostatic intermolecular interactions and/or hydrogen bonding to enhance the sensing ability of the thin film sensor material.[12] They are very stable for thin film formation and can be deposited onto a solid substrate using the spin-coating technique. Thin film sensor elements produced by Schiff base materials provide highly sensitive and reproducible responses against VOCs, in the field of environmental safety,[13,14] industrial monitoring,[10,15] and medical applications.[16,17] Therefore, they offer significant potential for the room temperature sensing elements by utilizing their amphiphilic nature, conjugated systems, and sensitivity to VOCs.[18]

In this study, chloroform vapor is selected to study the sensing properties and adsorption dynamics of Schiff base materials because of its molecular structure, which allows for dispersion forces and dipole–dipole interactions. The polarity difference between the carbon–chlorine and carbon–hydrogen bonds yields a dipole moment, which can create strong interactions (dipole–dipole interactions or hydrogen bonds, etc.,) between chloroform vapor and sensor material containing polar functional groups. Additionally, chloroform vapor can adsorb to the thin film structure, leading to molecular rearrangements or morphological changes due to its volatility. SPR technique enables us to study the molecular interactions between the thin film sensing material and the target gas or vapor molecules. It is used to determine optical parameters (refractive index and/or thickness) of thin films and to monitor the real-time sensor response against target molecules. It is widely used for chemical sensing applications because of changes in the film thickness and/or the refractive index values, which are evaluated by exciting a surface plasmon at the metal-dielectric thin film interface.[19,20] The SPR signal is highly sensitive to refractive index and film thickness changes. These advantages allow us to have fast online real-time detection with relatively short response times. In addition, the SPR technique is suitable for developing a low-cost, high-resolution, and fast-response chemical sensor.[21]

As the main purpose of this work along with the inconvenience of being limited number of papers available in the literature on VOC sensors with Schiff base using SPR measurement technique, two new Schiff base materials were synthesized and studied as a sensitive vapor sensor that may open a new strategy for exploring a set of new and responsive materials toward vapor sensor applications. To synthesize two novel Schiff base materials, 4-aminobenzoic acid (PABA) and 4-hydroxybenzoic acid (PHBA) molecules were chosen in this study. PABA is an isomeric form of aminobenzoic acid with carboxylic and amine functional groups. It can exist in

[a] *R. Çapan, D. Öğrence*
Science&Literature Faculty, Physics Department, Balikesir University, Balikesir, Turkey
E-mail: rcapan@balikesir.edu.tr

[b] *H. Namli*
Science&Literature Faculty, Chemistry Department, Balikesir University, Balikesir, Turkey

three forms depending on the pH of the environment (neutral, anion, and cation) and is a common ligand that binds to metal ions. Therefore, PABA has gained medical attention in the last decade.[22] PHBA is a *p*-hydrazinobenzoic acid, a hydrazine derivative of benzoic acid. The antioxidant properties of hydrazinobenzoic acid derivatives were evaluated through various in vitro methods, including the DPPH assay, and further supported by theoretical DFT calculations, indicating significant free radical scavenging potential.[23] Using PABA and PHBA molecules, two Schiff base materials were synthesized, namely, [(E)-4-((4-(dimethylamino)benzylidene)amino)benzoic acid (**DMPABA**) and (E)-4-(2-(4-(dimethylamino)benzylidene)hydrazinyl)benzoic acid (**DMPHBA**)]. **DMPABA** integrates a hydrophilic —COOH group with a hydrophobic dimethylamino-aromatic moiety, allowing its interaction with organic compounds. A spin coating film fabrication system was employed to prepare thin film sensors of **DMPABA** and **DMPHBA** materials. The SPR measurement system is used to collect the data during the interaction between chloroform vapor and the sensing element. The Elovich model is chosen to investigate the adsorption dynamics of **DMPABA** or **DMPHBA** sensor materials. The synthesis process and organic vapor sensing properties of spin-coated thin films using two novel **DMPABA** and **DMPHBA** materials have been demonstrated here.

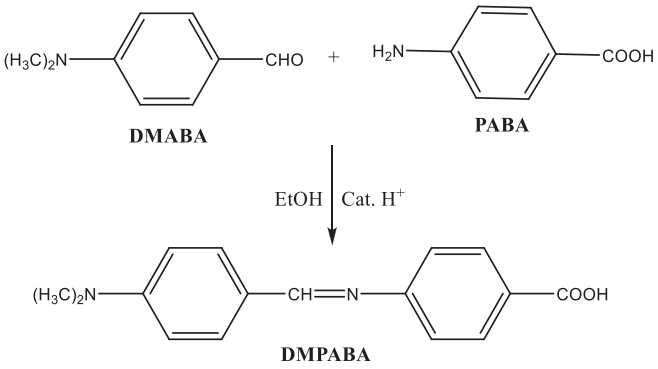

Scheme 1. Synthetic route to **DMPABA**.

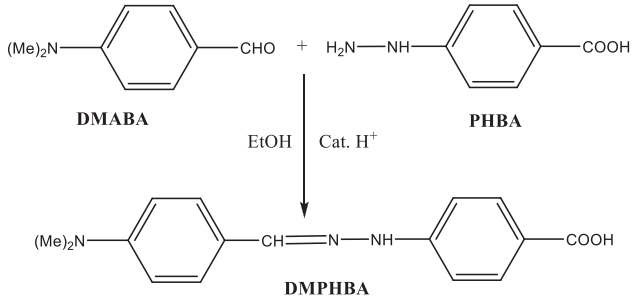

Scheme 2. Synthetic route to **DMPHBA**.

2. Materials and Methods

Chemicals involved in this study were purchased from Aldrich or Alfa Aesar and used as received without further purification. The ground-state geometries were optimized using density functional theory (DFT) with the B3LYP hybrid functional at the basis set level of 6-31G. The calculations were performed using the Gaussian 09 package.[24] The FTIR-ATR spectra were recorded on a Perkin Elmer Spectrum 65 spectrophotometer attached with ATR equipment.

Chloroform (99% Sigma-Aldrich) was used without further purification as the source of organic vapor for the **DMPHBA** and **DMPABA** thin film sensor preparations and SPR experiments. The vapor amount in ppm was calculated using Equation (1):[25]

$$c = \frac{22.4\rho V}{MV_0} x10^6 \quad (1)$$

where c (ppm) is the vapor concentration, V (mL) is the VOC volume, ρ (gmL^{-1}) the VOC density, M (gmol^{-1}) is the VOC molecular weight of material and V_0 (~0.02 mL) is the volume of the gas cell.

2.1. Synthesis of DMPABA

The **DMPABA** Schiff base (Scheme 1) was synthesized through a condensation reaction between 4-(dimethylamino)benzaldehyde and *p*-aminobenzoic acid. In a typical procedure, *p*-aminobenzoic acid (0.69 g, 5.00 mmol) and 4-(dimethylamino)benzaldehyde (0.75 g, 5.00 mmol) were dissolved in absolute ethanol (25 mL). The reaction mixture was heated under reflux for 4 h with continuous stirring. Upon cooling to room temperature, a bright yellow precipitate formed, which was collected by vacuum filtration and thoroughly washed with cold ethanol. The crude product was obtained in 83% yield (0.78 g). Final purification was achieved by recrystallization from acetonitrile, yielding 0.56 g (60% recovery) of pure **DMPABA** compound as yellow crystals.[26]

2.2. Synthesis of DMPHBA

Scheme 2 gives the synthesis process of **DMPHBA**. 4-Hydrazinobenzoic acid (0.69 g, 5.00 mmol, MW = 137.14 gmol^{-1}) and 4-(dimethylamino)-benzaldehyde (0.75 g, 5.00 mmol, MW = 149.19 g mol^{-1}) were dissolved in absolute ethanol (25 mL). Two drops of acetic acid were added to the solution. The reaction mixture was heated under reflux with continuous stirring for 4 h. After the reaction was complete, the mixture was cooled to room temperature. This resulted in the formation of a bright yellow–orange precipitate. The product was filtered and thoroughly washed with cold ethanol, then crystallized from ethanol.

2.3. Comparative FTIR Spectral Analysis

A comparative FTIR spectrum of the starting materials and the product is presented in Figures 1 and 2. As seen in Figure 1, the top spectrum (Figure 1a), corresponding to **DMABA**, the aldehy-

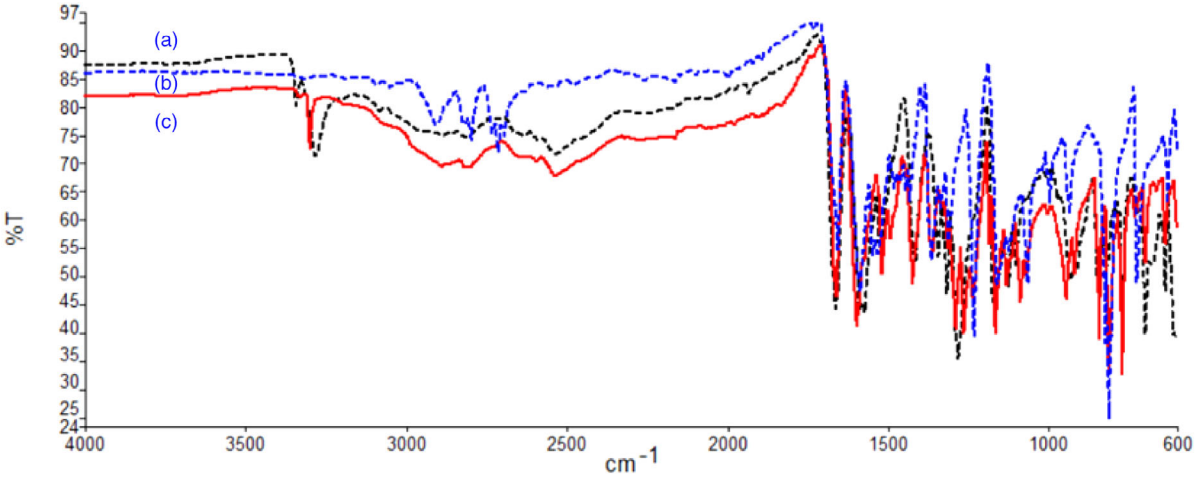

Figure 1. FTIR spectra of a) **PABA**, b) **DMABA**, and c) **DMPABA**.

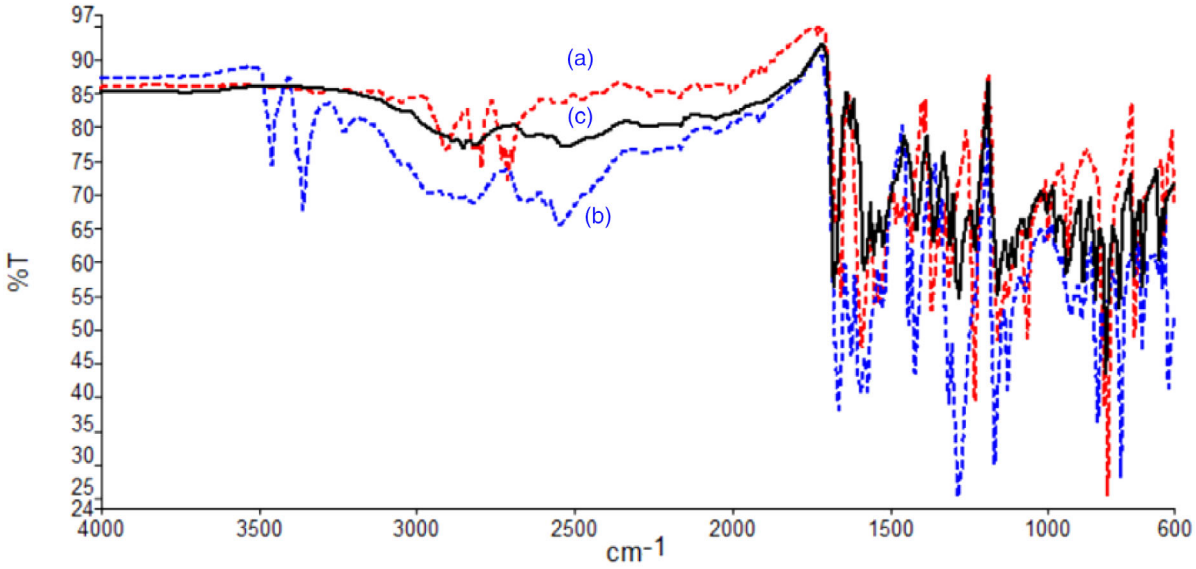

Figure 2. FTIR spectra of, a) **PHBA**, b) **DMABA**, and c) **DMPHBA** materials.

dic C—H stretch of the —CHO group is observed at 2904 cm^{-1}, the asymmetric and symmetric C—H stretching vibrations of the —CH_3 groups attached to the nitrogen atom appear in the range of 2795–2695 cm^{-1}, and the aldehydic carbonyl (C═O) group is detected at 1667 cm^{-1}.

In the middle spectrum, which corresponds to the product, the disappearance of the aldehyde C═O peak and the appearance of a C═C double bond stretching vibration at 1579 cm^{-1} are observed. Furthermore, in the bottom spectrum (Figure 1c) of PABA, the asymmetric and symmetric —NH^{-1} stretching bands at 3360 cm^{-1} (Figure 1b) disappear after the reaction, and the carbonyl peak of the newly formed Schiff base (COOH group) appears at 1675 cm^{-1}. In Figure 1c, which corresponds to the product, the disappearance of the aldehyde C═O peak of PABA and the appearance of a C═C double bond stretching vibration at 1579 cm^{-1} are observed.

By examining the comparative FTIR-ATR spectra of a) **PHBA**, b) **DMABA**, and c) **DMPHBA** shown in Figure 2, asymmetric and symmetric N—H stretching peaks at 3342 cm^{-1}, corresponding to the hydrazine —NH_2 group, are observed in the PHBA spectrum in Figure 2a. The observation of a single N—H stretch in the product **DMPHBA** indicates that the other hydrogens on the —NH_2 group were involved in the formation of the —C═N— imine bond, and the N—H stretching have disappeared. Additionally, the C═N double bond stretch at 1598 cm^{-1} is clearly observed in the **DMPHBA** spectrum in Figure 2c. Furthermore, the disappearance of the **DMABA** carbonyl peak at 1657 cm^{-1} in Figure 2b is a clear indication of imine formation.

2.4. Gaussian Periodic Boundary Conditions (PBC) Calculations for Molecular Geometry and Three-Dimensional (3D) Analysis of DMPABA

The **DMPABA** molecule was energy-minimized using MM2 in ChemBio. 3D, then further optimized for energy and 3D molecular geometry using Gaussian 09.

Research Article
doi.org/10.1002/slct.202503439
Chemistry Europe
European Chemical Societies Publishing

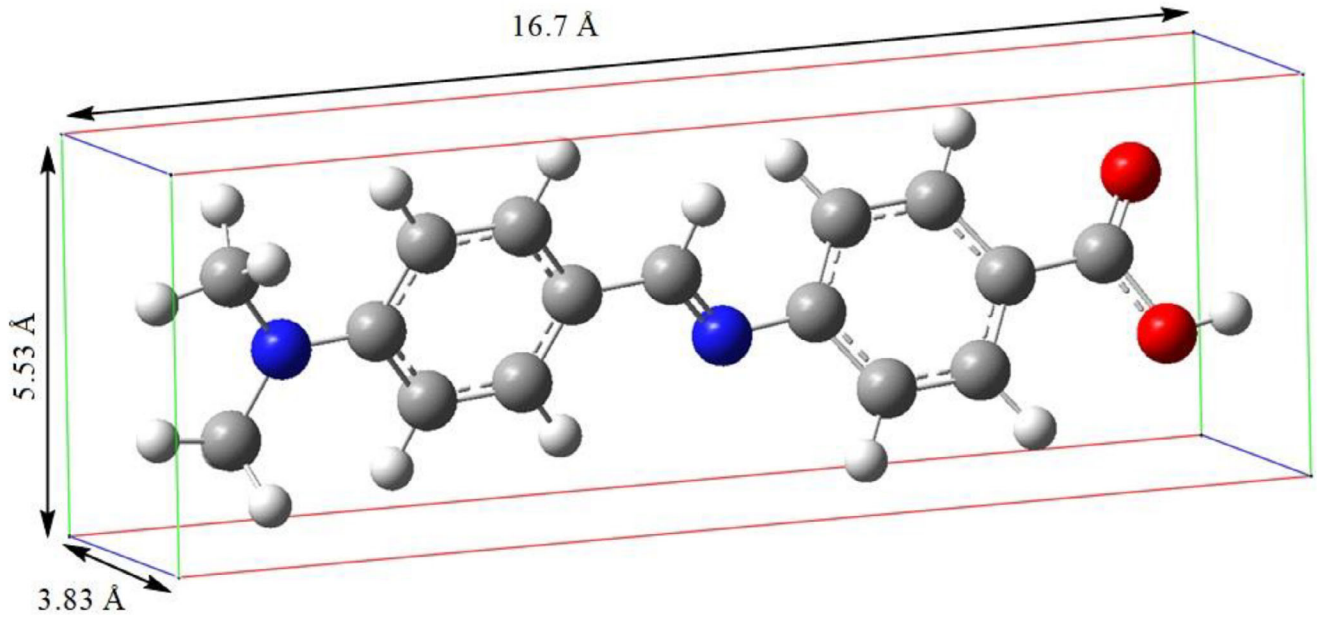

Figure 3. Calculated PBC for **DMPABA**.

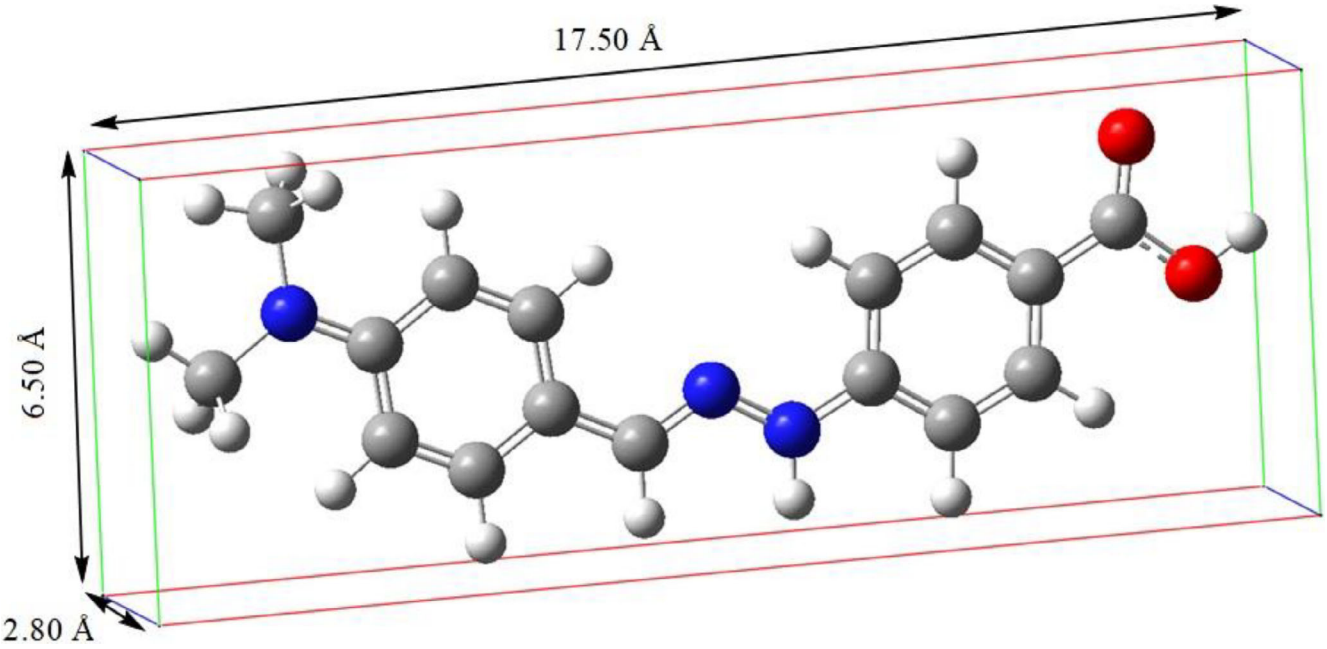

Figure 4. Calculated PBC for **DMPHBA**.

According to Gaussian Periodic Boundary Conditions (PBC) calculations, the molecular geometry and 3D analysis are as follows. The lattice parameters *a*, *b*, and *c* of **DMPABA** material shown in Figure 3 were calculated to be 16.7, 5.53, and 3.83 Å, respectively. The **DMPABA** molecule has a larger width than the **DMPHBA** molecule due to its nonplanar structure and the angle between the aromatic ring planes. These values are consistent with those measured in films prepared by the spin-coating technique.

2.5. Gaussian Periodic Boundary Conditions (PBC) Calculations for Molecular Geometry and 3D Analysis of DMPHBA

The energy and molecular geometry optimization of **DMPHBA** have been performed in the same manner (shown in Figure 4) as for **DMPABA**, and the 3D length, width, and breadth values of the molecule are provided below. In the related molecule, unlike **DMPABA**, both aromatic rings lie in the same plane. Due to the planarity of the molecule, its width (2.8 Å) is smaller than that of

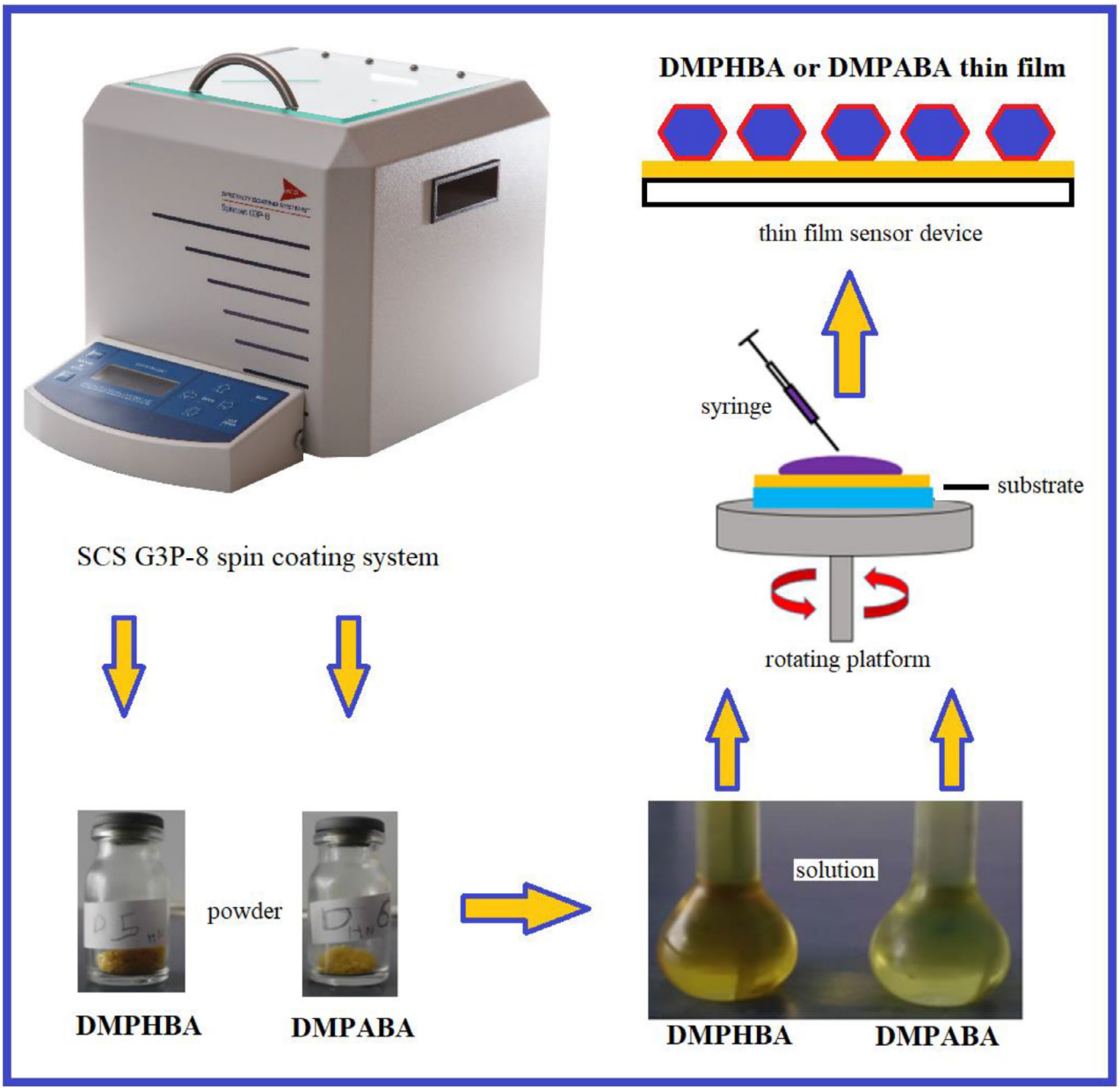

Figure 5. Thin film fabrication process for **DMPHBA** and **DMPABA** materials.

DMPABA (3.8 Å). The presence of an additional —NH— group in the **DMPHBA** molecule enhances its flexibility and leads to the conjugation of all double bonds across the molecule.[27]

2.6. Spin Coating Thin Film Fabrication

For a sensor application, the spin coating thin film technique is a very convenient method to produce thin film sensors by dropping a solution of the molecule onto a rotating solid substrate, which is rotated at a fixed spin speed to allow the solution spread onto the substrate to form a thin film with the help of the centrifugal force.[28] An SCS G3P-8 spin coating system (Figure 5) was employed for the fabrication of the **DMPHBA** and **DMPABA** thin film sensor devices.

The spin coating system has a plastic part on top of the device, which helps to isolate the thin film fabrication part from the environment. Thin films can be fabricated in a dust-free place. There is an electronic control unit on the front of the device. This unit helps us to control the rotation speed and the duration time of the thin film fabrication process. 12 mg of **DMPHBA** in a mixed solvent (10 mL chloroform and 1 mL methanol), 13 mg of **DMPABA** in a 10 mL chloroform solvent were used to prepare solutions. 50 nm thick gold-coated glass substrates with dimensions of 20 mm × 20 mm were supplied from TEKNOTIP company in TURKEY. Each substrate was separately replaced into the SCS G3P-8 spin coating system and was rotated at a spin speed value of 2000 rpm. 200 µL of **DMPHBA** and **DMPABA** solutions were separately dropped onto the substrate using a microliter syringe. Each substrate was rotated for

Research Article
doi.org/10.1002/slct.202503439
Chemistry Europe
European Chemical Societies Publishing

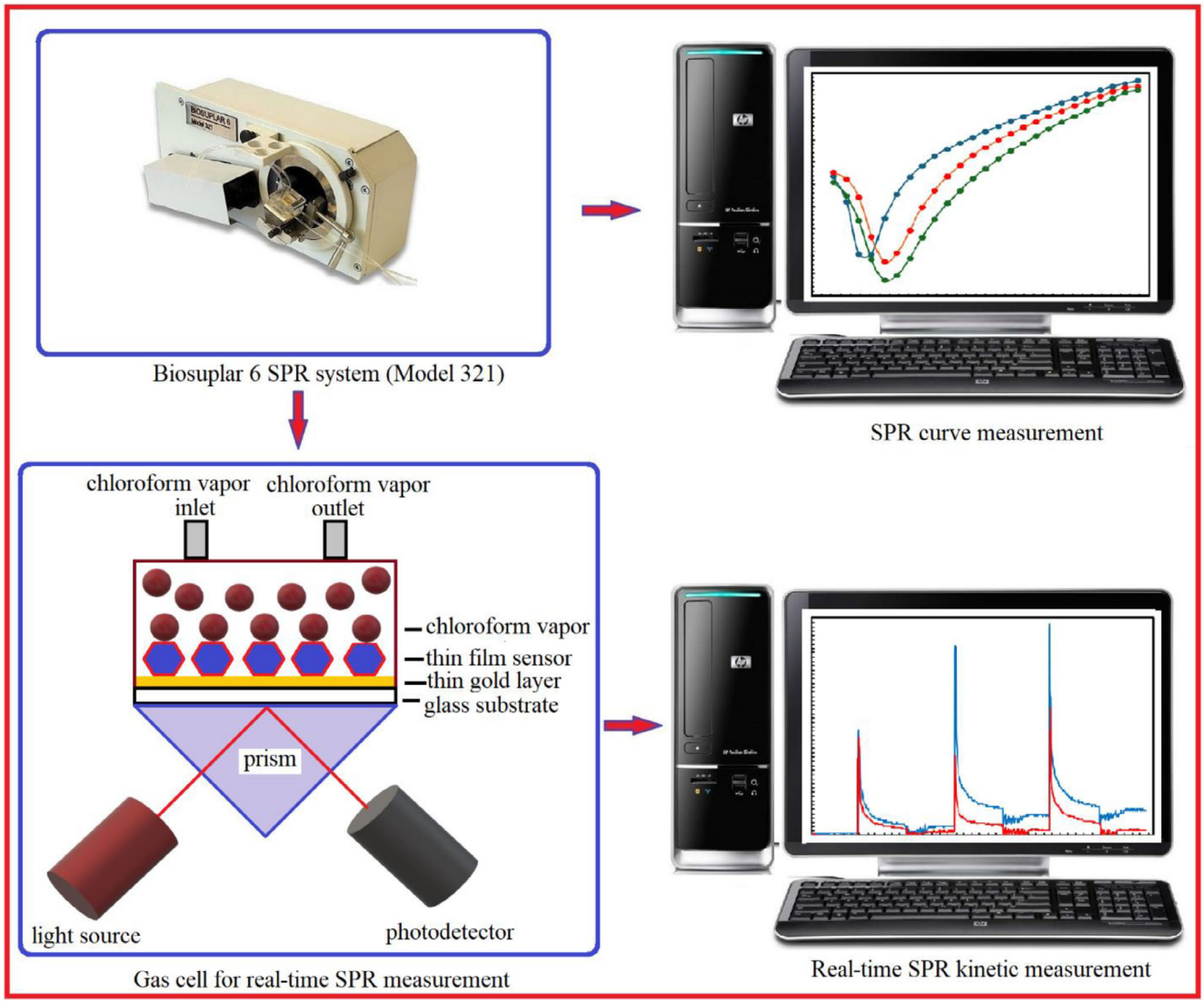

Figure 6. SPR measurement system.

the total thin film formation time of 60 s. After the rotation process stopped, 30 min were left for the thin film to evaporate any residual solvent, which may collapse in the **DMPHBA** and **DMPABA** thin film structure.

2.7. SPR Measurement System

The SPR system is suitable for investigating optical properties and sensor applications of thin films.[29] Figure 6 shows the SPR measurement system (BIOSUPLAR 6 Model spectrometer) and a schematic diagram of the gas cell.

To study optical parameters, Biosuplar software was enabled to collect data of the reflected light intensity against incidence angle with an approximately 0.003-degree angular resolution. The light source was a low-power (630–670 nm) laser diode. A gold-coated glass slide was placed onto a glass prism ($n = 1.51$). An optical contact between the glass slide and the prism was made using ethyl salicylate as an index-matching fluid. The prism was then mounted onto a holder within the SPR equipment. When the polarized laser beam interacted with a 50 nm gold thin layer and the interface between the thin gold surface and its coating of either the **DMPHBA** or **DMPABA** thin film, a total internal reflection occurred. The delocalized electrons at the surface of the gold thin layer were excited, leading to a surface plasmon resonance if the incidence is greater than the critical angle. It caused an adsorption of energy, leading to a sharp reduction in the reflected light intensity. When this happened, the angle is called the SPR resonance angle. Winspall fitting software [20] was applied to the SPR experimental data used to calculate refractive index and thickness values of the **DMPHBA** and **DMPABA** thin films.

The SPR system was also used for vapor sensor measurements. The real-time SPR kinetic measurement monitored the light intensity at a fixed angle (θ) versus time (t) whilst interactions between **DMPHBA** or **DMPABA** thin films and the chloroform vapor. A gas cell was constructed out of transparent plastic and contained an outlet and an inlet, which were both fitted

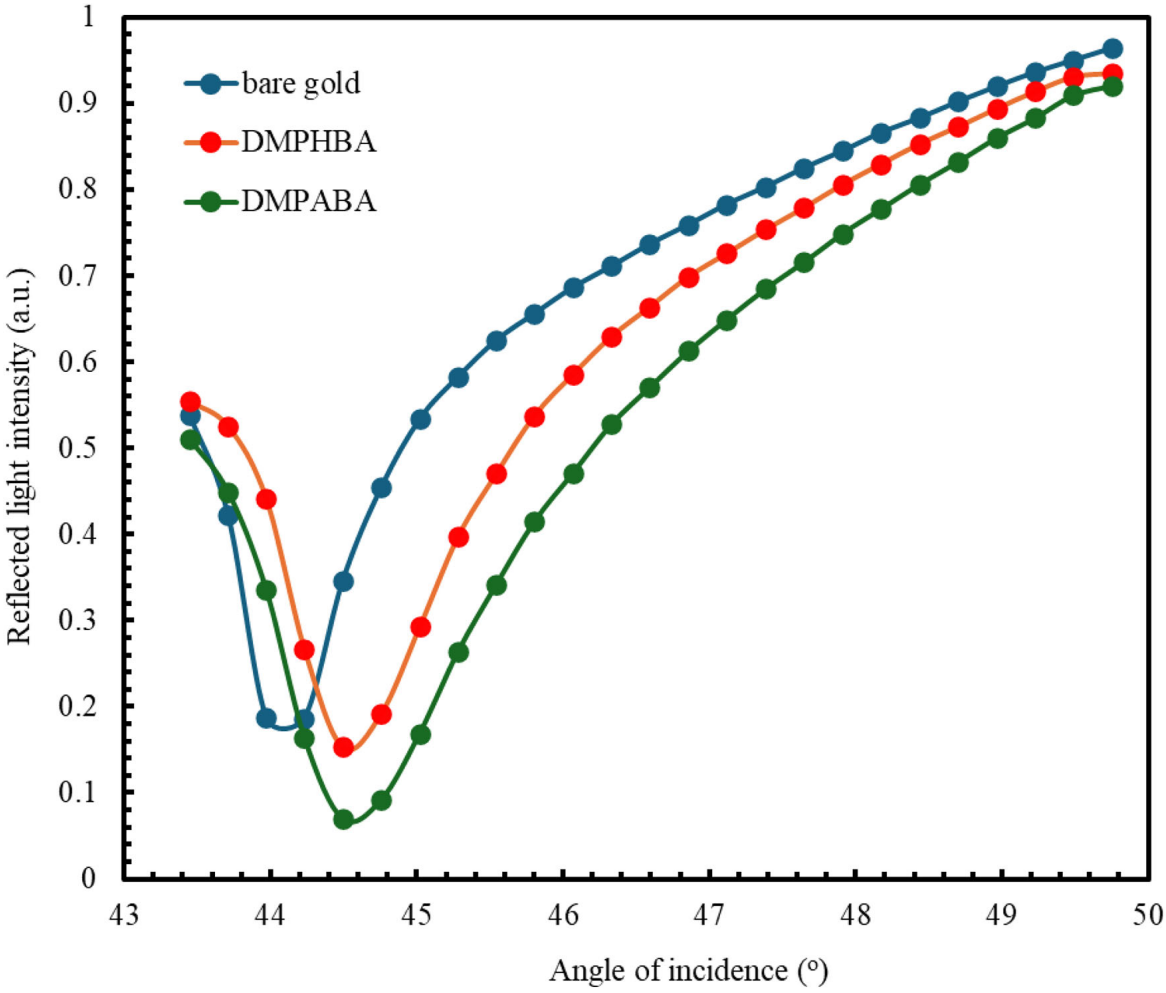

Figure 7. SPR results of **DMPHBA** and **DMPABA** thin films with experimental data and fitting graphs.

with silicone tubes. The gas cell had an inlet and an outlet connected to silicone tubes. The **DMPHBA** or **DMPABA** thin films were replaced between the gas cell and the prism. A syringe was used to inject the chloroform vapor or dry air into the gas cell. The Elovich Model was applied to SPR kinetic measurements to elucidate the adsorption dynamics between the **DMPHBA** and **DMPABA** thin films and chloroform vapor molecules.

3. Results and Discussion

Figure 7 shows the reflected light intensity at varying angles of incidence for bare gold, **DMPHBA**, and **DMPABA** thin films. It is very noticeable that the SPR curves for both films indicate an angle shift from the SPR curve for the bare gold. Angle shifts can be explained by the fact that both materials are suitable for producing a sensor element. The SPR curve of **DMPHBA** yielded a similar angle shift to the SPR curve of **DMPABA** thin film, depending on optical parameters such as the refractive index (n) and the thickness (d) of the thin films. WINSPALL fitting software was applied to the SPR experimental data to determine the refractive index and thicknesses of **DMPHBA** and **DMPABA** thin films. The refractive index values for both thin films are determined to be 1.47. The thickness values of **DMPHBA** and **DMPABA** thin films are estimated to be 19.7 ± 0.1 and 21.7 ± 0.1 Å, respectively. As seen in Figures 3 and 4, these values are in good agreement, with the computationally determined maximum lengths being 17.50 and 16.70 Å.

Time-dependent SPR kinetic measurement is important to investigate the sensor behavior between the sensing element and VOC molecules. Figure 8 shows three SPR kinetic cycles when **DMPHBA** and **DMPABA** thin filmswere exposed to saturated chloroform vapor. The similarity in the response of these three cycles shows the stability and reproducibility of sensor responses.

The initial stage in time-dependent SPR kinetic measurements is to flush dry air as a reference gas through **DMPHBA** and **DMPABA** thin films to achieve a baseline from 0 to 120 s. 3 mL of chloroform vapor was injected with an injector into the gas cell at 120 s. There is an initial sharp increase in reflected light intensity as the vapor molecule is adsorbed into both thin film structures. The reason for the sharp increase is possibly because the film is actively binding the chloroform vapor molecules. This can be explained by the adsorbing vapor molecules moving into the thin film structure and increasing the film transparency,

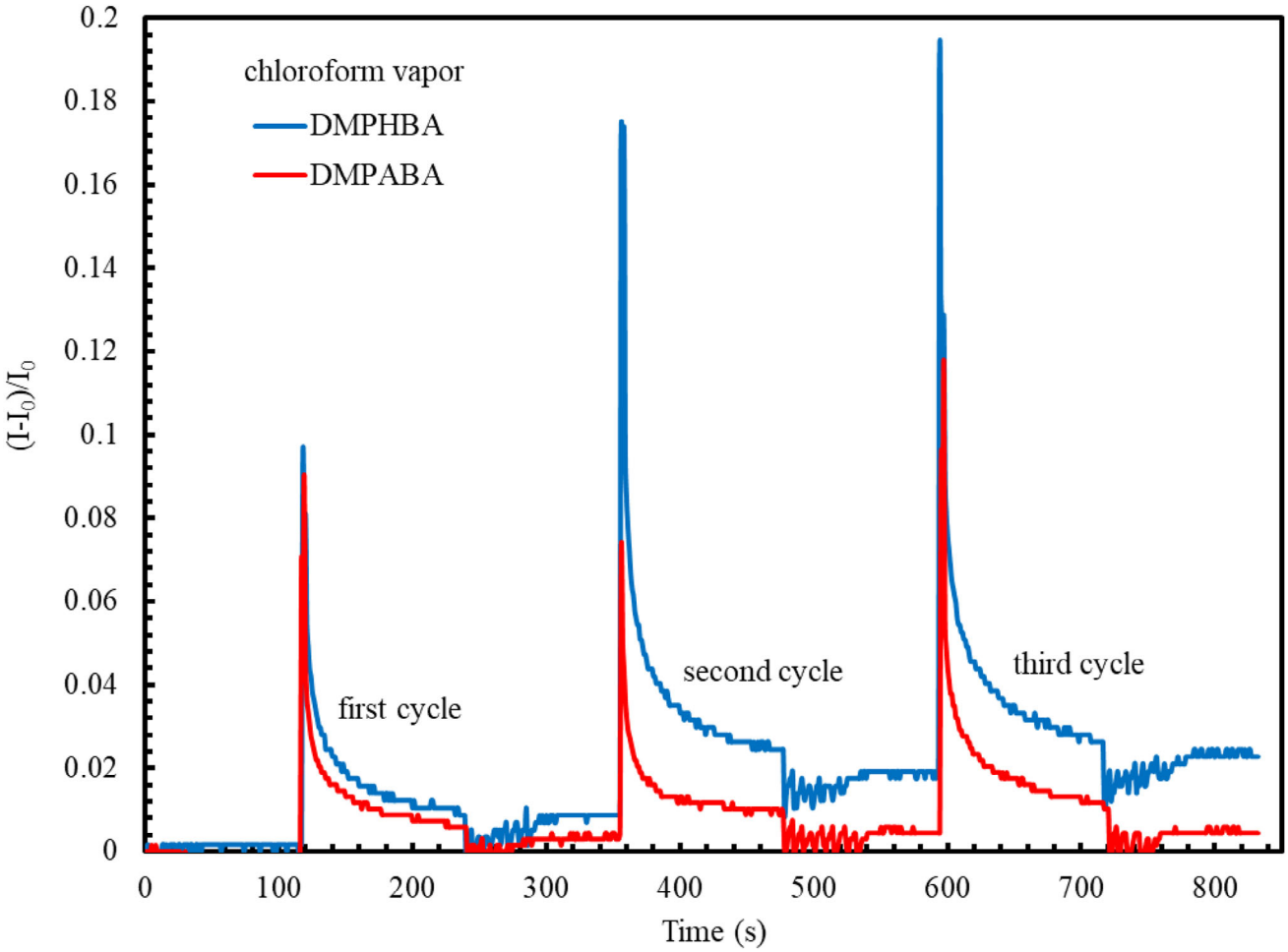

Figure 8. Real-time SPR kinetic measurements of the **DMPHBA** and **DMPABA** thin films.

Table 1. Sensor properties for **DMPHBA** and **DMPABA** thin films against chloroform vapor.

	Cycle	t_{res} (response time)	t_{rec} (recovery time)	I_i (the reflected light intensity at the initial stage)	I (the reflected light intensity during the vapor interaction stage)	$\Delta I = I\text{-}I_i$	$\Sigma \Delta I$ (mean value)
DMPHBA	1	1.404	4.210	570.939	577.988	7.049	8.38
	2	1.952	6.829	574.951	585.941	10.99	
	3	1.951	2.936	580.891	588.02	7.129	
DMPABA	1	1.064	4.878	686.931	695.049	8.118	6.93
	2	1.701	6.829	690.297	696.04	5.743	
	3	2.67	5.854	691.089	698.02	6.931	

causing rapid changes in the film thickness and structure, followed by the film settling down and reaching equilibrium. This change drops and tends toward a constant value with time as the film stabilizes. Upon flushing with dry air between 120 and 240 s, if **DMPHBA** and **DMPABA** thin film sensors have a reversible response, the sensor response approaches the initial baseline with a decrease in the reflected light intensity. On flushing with dry air at 360 s, the reverse desorption of chloroform vapor occurs, again with an initial sharp peak where desorption is most rapid, followed by a slower trend to the initial state. Dry air/chloroform vapor process to both thin films was repeated three times from the beginning of the measurements to the end of the measurements using 120 s time intervals. **DMPHBA** and **DMPABA** thin films gave a reversible response to chloroform vapor. However, the reversibility of the **DMPABA** thin film is better than **DMPHBA** thin film in returning to the initial state. The numerical calculations of sensor parameters for **DMPHBA** and **DMPABA** thin films, as determined using Figure 8, are given in Table 1. **DMPHBA** thin film indicates a higher response than **DMPABA** thin film.

It is well known that the chemical structure of the selected material plays an important role, such as hydrogen binding,

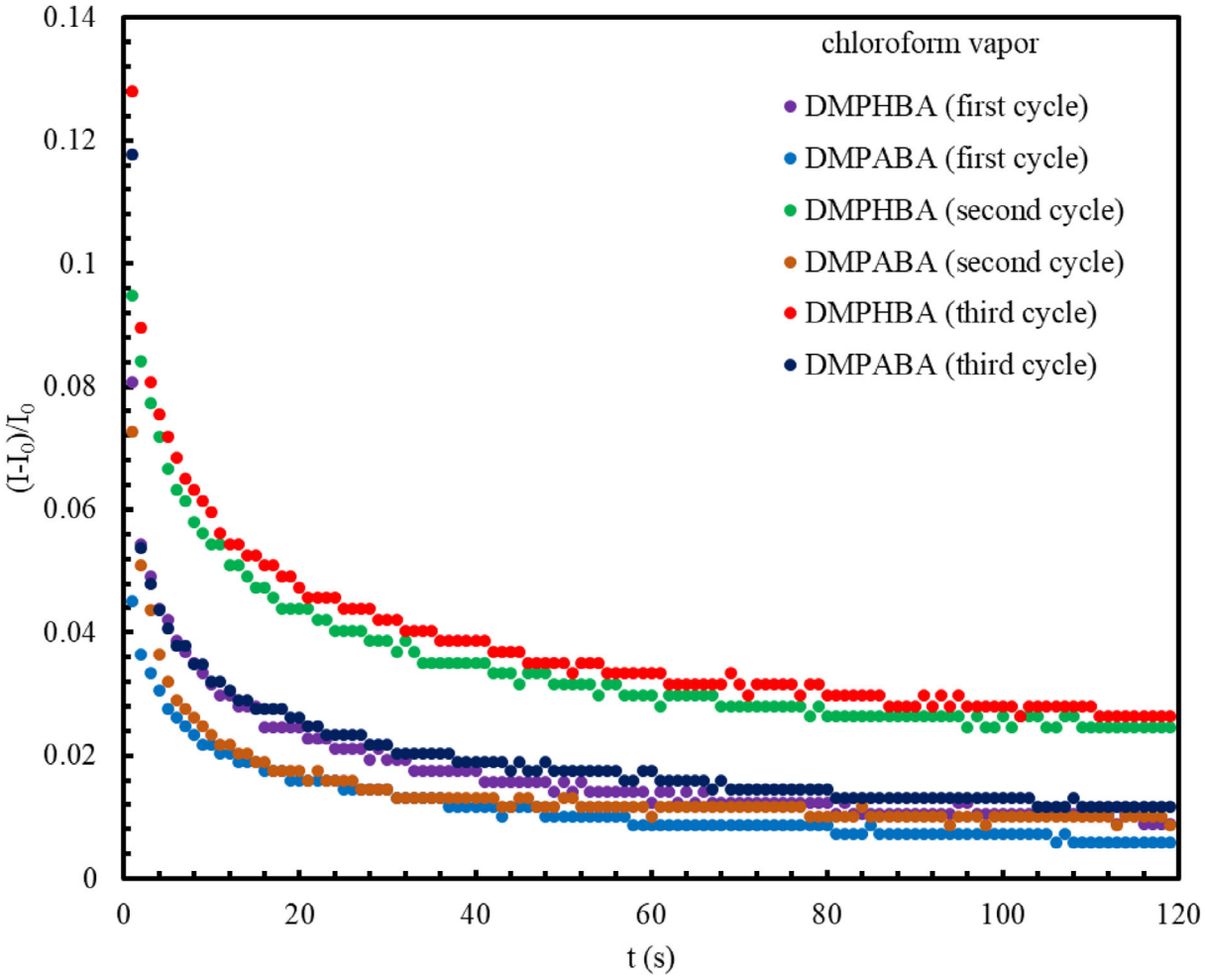

Figure 9. SPR responses for the **DMPHBA** and **DMPABA** thin films as a function of time.

dipole–dipole, and Van der Waals interactions[30,31] in designing vapor sensors of a highly sensitive thin film layer to design against VOCs detection.[32]

The chemical formula of **DMPHBA** ($C_{16}H_{17}N_3O_2$) and **DMPABA** ($C_{16}H_{16}N_2O_2$) materials have a very similar structure. The difference between the two materials is an extra —NH— group in the **DMPHBA** material. As a result of this, the molecular weight of **DMPHBA** (268 $gmol^{-1}$) is higher than the molecular weight of **DMPABA** (283 $gmol^{-1}$). Both materials have aromatic groups with a benzene ring and the carboxyl (—COOH) group, which are suitable for gas/vapor sensing applications when the —NH— group is added to **DMPHBA** material. According to the response rate in Table 1, **DMPHBA** thin film demonstrates a higher response than **DMPABA** thin film when they are exposed to chloroform vapor at the same laboratory conditions. It can be explained that one of the strongest could be the formation of hydrogen bonds between **DMPHBA** thin film and the chloroform vapor molecules. Basova et al investigated the interactions of phthalocyanine films with organic vapors using Raman spectroscopy. The Raman spectra proved the formation of hydrogen bonding interactions between the side chains of the phthalocyanine moieties and electron-donating atoms (O, Cl) within a range of vapor molecules.[30] Within this study, similar interactions between the chloroform vapors and **DMPHBA** thin film have the formation of hydrogen bonds between guest and host.

In order to analyze a sensor interaction, the adsorption process between the thin film and target adsorbent is another sensing interaction factor that must be investigated. In an adsorption feature, the adsorbate encounters the surface, interacts with the surface, and then migrates into the film structure. Linear or nonlinear adsorption models, such as Pseudo-first order and Pseudo-second order models, Ritchie and Elovich models, can be developed to analyze an adsorption process using time-dependent SPR data.[33] These models allow us to determine the sorption capacity, the rate of adsorption, the suitability of fitting parameters, and the correlation coefficient. In this study, the Elovich model is selected to investigate the adsorption dynamics by using the correlation coefficient (R^2) as an indicator of the conformity between the model prediction and the experimental adsorption data.

To understand the adsorption mechanism and to calculate the interaction parameters of chloroform vapors with the **DMPHBA** and **DMPABA** thin films, the data in Figure 8 (from 120 to 240 s, from 360 to 480 s, from 600 to 720 s) for each cycle is selected from the initial point of vapor injection to the end of the interaction. The data indicating the change in the SPR

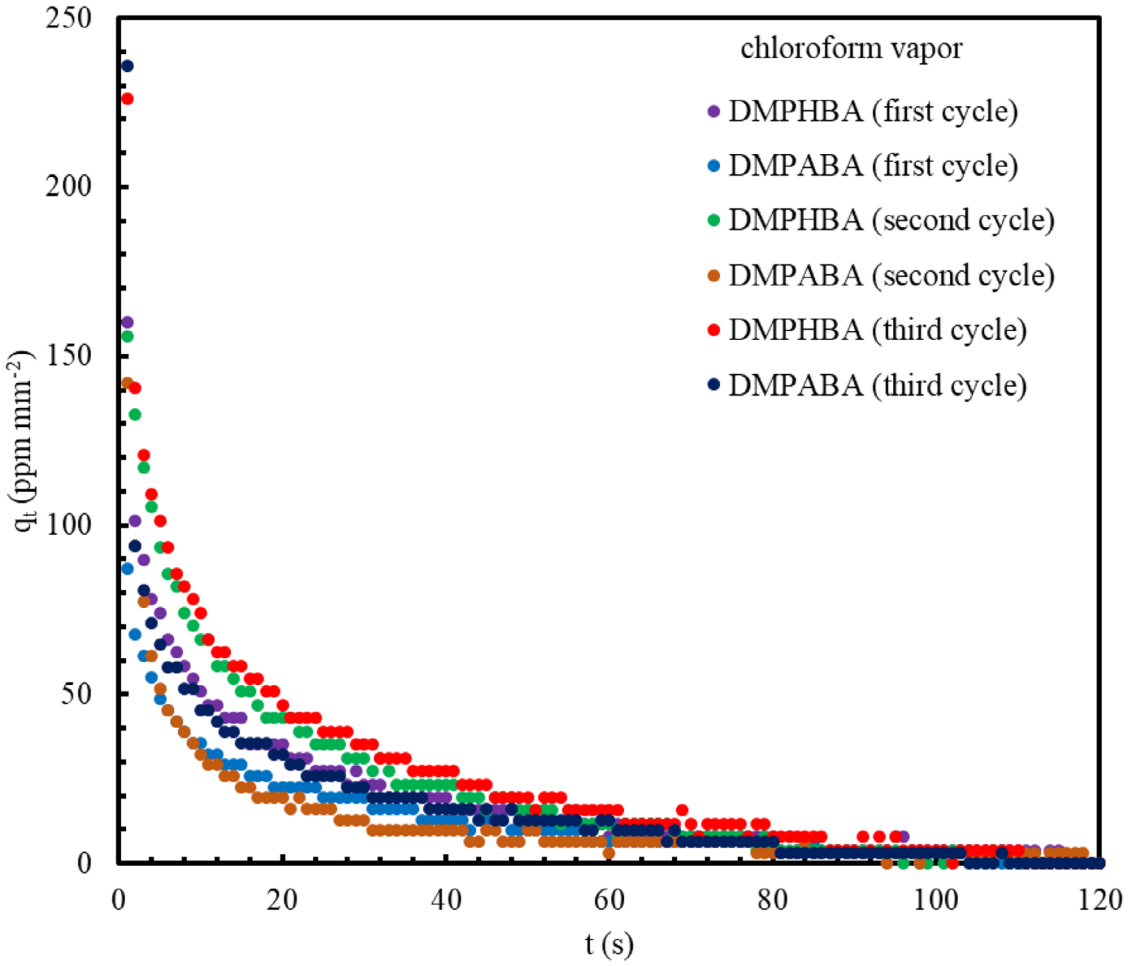

Figure 10. q_t values for the **DMPHBA** and **DMPABA** thin films as a function of time.

response in time during the exposure to the vapor with a duration of 2 min was plotted in Figure 8. The graph of the $\frac{(I-I_0)}{I}$ value against time is given in Figure 9, and the vapor molecules were exposed in 3 cycles using the same saturated concentration.

While the vapor adsorption to the thin film sensor increases rapidly at first, the adsorption slows down over time and finally reaches an equilibrium.[34] The probability of adsorption of a vapor molecule decreases exponentially as a function of the number of vapor molecules that have already adsorbed onto the surface.[35] The sorption capacity, q_t, for the SPR measurement is described as:[33]

$$q_t = \left[\frac{(I_i - I_e)V}{A}\right] \quad (2)$$

where I_i is the initial reflected light intensity, I_e is the equilibrium reflected light intensity, V is the injected vapor volume, and A is the thin film surface area, respectively. Using Figure 9 and Equation (2), q_t is calculated and presented as a function of time in Figure 10.

The model states that the speed of the adsorption process (dq_t/dt) onto a film structure depends on the amount of vapor adsorbed onto the surface. The sorption capacity, the initial adsorption rate, and the Elovich constant were calculated using the Elovich equation, which can be described as follows:[36]

$$\frac{dq_t}{dt} = aexp(-bq_t) \quad (3)$$

where qt represents the quantity of vapor molecules adsorbed at time t, a is the initial adsorption rate, and b is the Elovich constant. In the Elovich equation, constant a is regarded as the initial adsorption rate because (dqt/dt) approaches a when qt approaches zero. If the boundary conditions can be chosen from $q_t = q_t$ at $t = t$ and $q_t = 0$ at $t = 0$, Equation (3) is easily integrated. Wua described the final form of the Elovich equation as:[37]

$$q_t = \left(\frac{1}{b}\right) ln(ab) + \left(\frac{1}{b}\right) lnt \quad (4)$$

Equation (4) is used to test the applicability of the Elovich model to the kinetics of chloroform vapor adsorption onto the surface. The assumption of $t \gg t_0$ and validity of Equation (4) is checked by plotting q_t versus ln t. The plot of q_t versus ln t would yield a linear relationship, which can be used to determine the values of a and b using the slope ($\frac{1}{b}$) and the intercept ($\frac{1}{b}$)$lnab$ of the plot, respectively.[38] The graph of q_t versus ln t for the **DMPHBA** and **DMPABA** thin films is given in Figure 11.

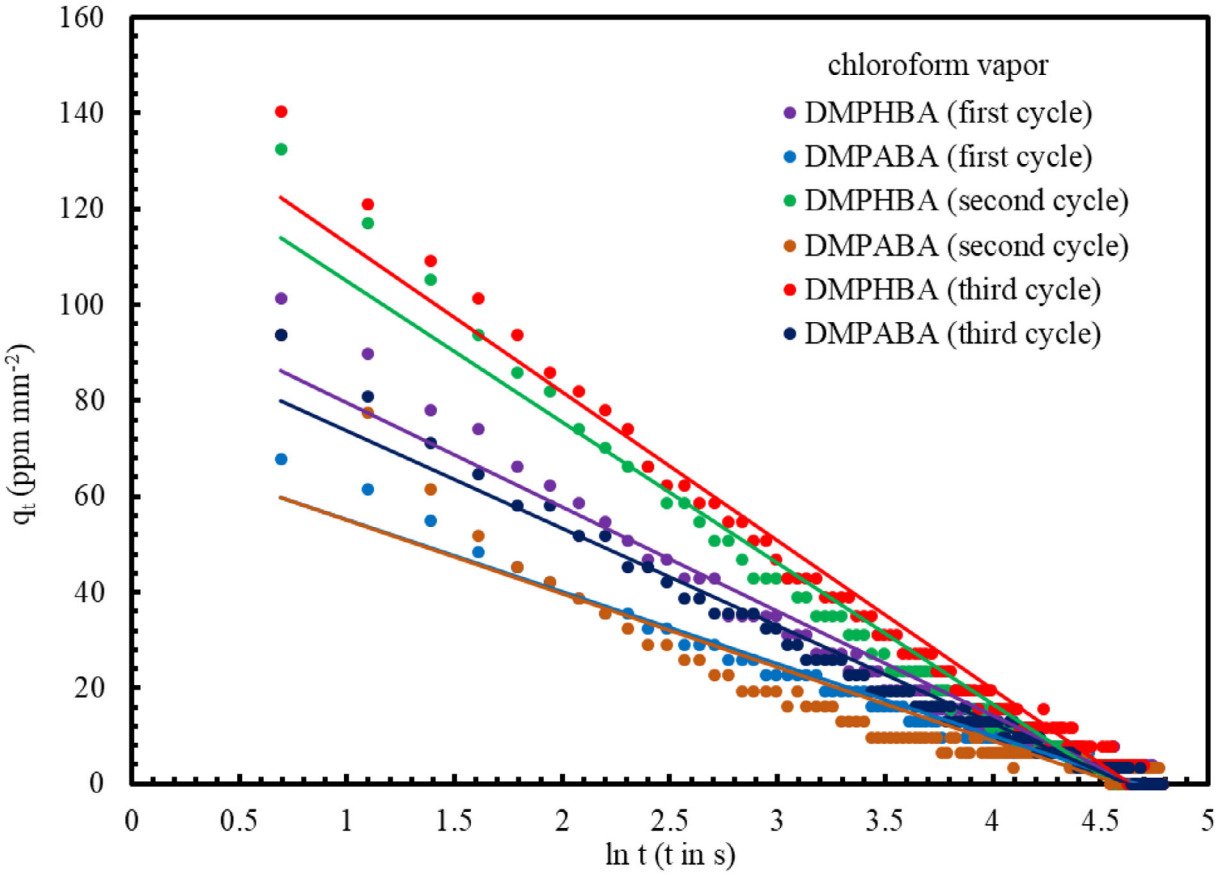

Figure 11. Elovich model adsorption graphs of the **DMPHBA** and **DMPABA** thin films.

Table 2. Calculated Elovich constants of the **DMPHBA** and **DMPABA** thin films.

Elovich model (DMPHBA)						
Cycle	a (ppm mm^{-2})	b (mm^{2}s ppm^{-1})	R^2	Mean value (a)	Mean value (b)	Mean value (R^2)
1st	2292.925	0.0459	0.965	2775.97	0.0373	0.972
2nd	2837.878	0.0339	0.971			
3rd	3197.108	0.0322	0.979			
Elovich model (DMPABA)						
Cycle	a (ppm mm^{-2})	b (mm^{2}s ppm^{-1})	R^2	Mean value (a)	Mean value (b)	Mean value (R^2)
1st	1610.846	0.0665	0.9782	1728.51	0.0602	0.935
2nd	1498.733	0.0651	0.8499			
3rd	2075.958	0.0491	0.9783			

Elovich constants (a, b, and R^2) for the **DMPHBA** and **DMPABA** thin films were calculated using Figure 11, and the calculated values are represented in Table 2.

It can be seen that all graphs have a linear relationship with fitting values of 0.972 for the **DMPHBA** and 0.935 for the **DMPABA** thin films. R^2 value of the **DMPHBA** material is higher than R^2 value of **DMPHBA** material due to adding the —NH— group to the **DMPHBA** molecular structure.

The value of a (the initial adsorption rate) is dramatically increased. The change of b (the Elovich desorption constant) value is reversed. It can be concluded that adding the —NH— group to the molecular structure yielded a high adsorption process for the detection of chloroform vapor.

4. Conclusions

Two Schiff base compounds (**DMPABA** and **DMPHBA**) were synthesized via a condensation reaction, and their chemical structures were confirmed by FTIR-ATR spectroscopy. Using the spin coating method, they successfully fabricated the **DMPHBA** and **DMPABA** thin films with thickness values of 19.7 ± 0.1 and

21.7 ± 0.1 Å, respectively. The sensor behavior and adsorption dynamics were investigated using the SPR technique. When the —NH— group was attached to the **DMPHBA** chemical structure, the sensor response was improved from 6.93 to 8.38. The adsorption dynamics of **DMPHBA** and **DMPABA** thin films during exposure to chloroform vapor were studied using the Elovich Model. The initial adsorption rates were determined to be 2775.97 ppm mm^{-2} for **DMPHBA** and 728.51 ppm mm^{-2} for **DMPABA**. The Elovich constant was calculated as 0.0373 $mm^2s\ ppm^{-1}$ for **DMPHBA** and 0.0602 $mm^2s\ ppm^{-1}$ for **DMPABA**. The **DMPHBA** molecule with an —NH— group may be considered as the reason why this molecule exhibits higher sensitivity to chloroform vapor compared to the **DMPABA** molecule. This study indicated that **DMPHBA** and **DMPABA** Schiff base thin films may be candidates for chloroform vapor sensing applications with their high adsorption features, stable, fast response, and reversibility.

Acknowledgments

The authors have nothing to report.

Conflict of Interests

The authors declare no conflict of interest.

Data Availability Statement

The data that support the findings of this study are available from the corresponding author upon reasonable request.

Keywords: Adsorption · Elovich model · Schiff bases · Sensors · Surface plasmon resonance

[1] M. G. Guilléna, J. R. F. Gámeza, T. L. Costaa, S. M. A. Pintob, M. J. F. Calveteb, M. M. Pereirab, J. M. Pedrosa, *Sens. Actuators B* **2018**, *260*, 116–124.
[2] T. Basova, *Chemosensors* **2024**, *12*, 56.
[3] I. Capan, M. Bayrakci, M. Erdogan, M. Ozmen, *IEEE Sens. J.* **2019**, *19*, 838–845.
[4] G. Liu, A. Abdurahman, Z. Zhang, Y. Feng, F. Li, M. Zhang, *Sens. Actuators B* **2019**, *296*, 126592.
[5] M. Kaur, S. Kumar, M. Yusuf, J. Lee, R. J. C. Brown, K. H. Kim, A. K. Malik, *Coord. Chem. Rev.* **2021**, *449*, 214214.
[6] R. Çapan, M. Erdoğan, I. Çapan, C. O. Erdoğan, F. G. Moscoso, J. M. Pedrosa, L. K. Komodiki, A. J. Tasiopoulos, *IEEE Sens. J.* **2022**, *22*, 18287–18294.
[7] E. Halay, S. Bozkurt, R. Capan, M. Erdogan, R. Unal, Y. Acikbas, *Res. Chem. Intermed.* **2020**, *46*, 4433–4445.
[8] S. Mirabella, I. P. Oliveri, F. Ruffino, G. Maccarrone, S. D. Bella, *Appl. Phys. Lett.* **2016**, *109*, 143108.
[9] L. Hou, X. Xu, X. Wang, L. Wang, F. Tian, Y. Xu, *J. Mater. Chem.* **2024**, *12*, 9817–9829.
[10] B. Musikavanhu, Y. Liang, Z. Xue, L. Feng, L. Zhao, *Mol.* **2023**, *28*, 6960.
[11] P. Loomba, S. B. Nallamalla, K. Suresh, J. M. Reddy, S. Rana, N. K. Katari, S. S. B. Manabolu, *J. Indian Chem. Soc.* **2025**, *102*, 101756.
[12] E. Halay, I. Capan, R. Capan, E. Ay, Y. Acikbas, *Res. Chem. Intermed.* **2024**, *50*, 4579–4593.
[13] V. Sharma, R. Chandra, S. Dutta, D. Sahu, G. K. Patra, *Inorg. Chim. Acta* **2024**, *573*, 122321.
[14] N. M. Sundar, A. K. Srinivasan, P. Keerthana, S. J. Stanley, G. A. Kumar, *Compos. Commun.* **2021**, *25*, 100750.
[15] M. A. M. Alhamami, A. Y. A. Mohammed, J. S. Algethami, H. M. Al-Saidi, S. Khan, S. S. Alharthi, *Microchem. J.* **2024**, *197*, 109817.
[16] P. Mishra, P. Sethi, S. Kumar, P. Rathi, A. Umar, R. Kumar, S. Chaudhary, A. A. M. Alkhanjaf, A. A. Ibrahim, S. Baskoutas, *J. Mol. Struct.* **2024**, *1317*, 139098.
[17] M. Shit, S. Halder, K. Manna, A. K. Karan, A. Samanta, N. B. Manik, S. Pal, K. Jana, C. Sinha, *ACS Appl. Poly. Mater.* **2024**, *6*, 2637–2648.
[18] R. Kumar, W. Zheng, X. Liu, J. Zhang, M. Kumar, *Adv. Mater. Technol.* **2020**, *5*, 1901062.
[19] I. Pockrand, *Surf. Sci.* **1978**, *72*, 577–588.
[20] A. K. Hassan, C. Goy, A. V. Nabok, *Thin Solid Films* **2008**, *516*, 9006–9011.
[21] C. Ozkaya, R. Capan, M. Erdogan, F. Ozcil, F. Yukruk, *Mol. Syst. Des. Eng.* **2020**, *5*, 1057–1070.
[22] V. Vinayagam, D. Chandren, P. Arthur, S. Theerthagiri, K. Velsankar, W. Yong, *Inorg. Chem. Commun.* **2024**, *161*, 112116.
[23] H. A. Abuelizz, H. A. A. Taie, A. H. Bakheit, G. A. E. Mostafa, M. Marzouk, H. Rashid, R. Al-Salahi, *ACS Omega* **2021**, *6*, 31993–32004.
[24] M. J. Frisch, G. W. Trucks, H. B. Schlegel, G. E. Scuseria, M. A. Robb, J. R. Cheeseman, G. Scalmani, V. Barone, B. Mennucci, G. A. Petersson, H. Nakatsuji, M. Caricato, X. Li, H. P. Hratchian, A. F. Izmaylov, J. Bloino, G. Zheng, J. L. Sonnenberg, M. Hada, M. Ehara, K. Toyota, R. Fukuda, J. Hasegawa, M. Ishida, T. Nakajima, Y. Honda, O. Kitao, H. Nakai, T. Vreven, J. A. Montgomery, et al., Gaussian 09, Revision D.01 ed., Gaussian, Inc., Wallingford CT, USA **2013**.
[25] X. Fan, B. Y. Du, *Sens. Actuators, B* **2012**, *166*, 753–760.
[26] P. Naik, D. D. Babu, S. Rui, A. El-Shafei, A. V. Adhikari, *Mater. Today: Proc.* **2018**, *5*, 3150–3157.
[27] O. A. Nurkenov, S. D. Fazylov, Z. B. Satpaeva, T. M. Seilkhanov, D. M. Turdybekov, A. Z. Mendibayeva, S. B. Akhmetova, Z. T. Shulgau, L. E. Alkhimova, I. V. Kulakov, *Chem. Data Collect.* **2023**, *5*, 3150–3157.
[28] M. D. Tyona, *Adv. Mater. Res.* **2013**, *2*, 195–208.
[29] L. Ji, Y. Chen, Y. J. Yuan, *Sens. Actuators, B* **2014**, *198*, 82–86.
[30] T. Basova, E. Koltsov, A. K. Ray, A. K. Hassan, A. G. Gurek, V. Ahsen, *Sens. Actuators, B* **2006**, *113*, 127–134.
[31] F. Benevelli, A. Bond, M. Duer, J. Klinowski, *Phys. Chem. Chem. Phys.* **2000**, *2*, 3977–3981.
[32] S. Kumar, S. Chawla, M. C. Zou, *J. Incl. Phenom. Macrocycl. Chem.* **2017**, *88*, 129–158.
[33] R. Capan, I. Capan, F. Davis, *Sens. Actuators, B* **2023**, *394*, 134463.
[34] D. Saha, H. A. Grappe, *Adsorption Properties of Activated Carbon Fibers, Activated Carbon Fiber and Textiles*, (Ed.: J. Y. Chen), Woodhead Publishing Elsevier, Sawston, Cambridge **2017**, pp. 143–165.
[35] T. H. Richardson, C. M. Dooling, L. T. Jones, R. A. Brook, *Adv. Colloid Interface Sci.* **2005**, *116*, 81–96.
[36] Ş. Altın, F. Dumludag, Ç. Oruç, A. Altındal, *Microelectron. Eng.* **2015**, *134*, 7–13.
[37] F. C. Wua, R. L. Tseng, R. S. Juang, *Chem. Eng. J.* **2009**, *150*, 366–373.
[38] M. Pişkin, N. Can, Z. Odabas, A. Altındal, *J. Porphyrins Phthalocyanines* **2018**, *22*, 189–197.

Manuscript received: June 13, 2025